AIAA 2003–3955

A continuous adjoint method for unstructured grids

Antony Jameson and Sriram
Dept of Aeronautics and Astronautics
Stanford University, Stanford, CA

Luigi Martinelli
Dept of Mechanical and Aerospace Engineering
Princeton University, Princeton, NJ

16th CFD Conference
June 23–26, 2003/Orlando, FL

A continuous adjoint method for unstructured grids

Antony Jameson *and Sriram
Dept of Aeronautics and Astronautics
Stanford University, Stanford, CA

Luigi Martinelli †
Dept of Mechanical and Aerospace Engineering
Princeton University, Princeton, NJ

Adjoint based shape optimization methods have proven to be computationally efficient for aerodynamic problems. The majority of the studies on adjoint methods have used structured grids to discretize the computational domain. Due to the potential advantages of unstructured grids for complex configurations, in this study we have developed and validated a continuous adjoint formulation for unstructured grids. The hurdles posed in the computation of the gradient for unstructured grids are resolved by using a reduced gradient formulation. Methods to impose thickness constraints on unstructured grids are also discussed. Results for two and three dimensional simulations of airfoils and wings in transonic flow are used to validate the design procedure. Finally, the design procedure is applied to redesign the shape of a transonic business jet configuration, and we were able to reduce the drag of the aircraft from 235 to 216 counts resulting in a shock free wing.

Introduction

With the availability of high performance computing platforms and robust numerical methods to simulate fluid flows, it is possible to shift attention to automated design procedures which combine CFD with optimization techniques to determine optimum aerodynamic designs. The feasibility of this is by now well established,[1–6] and it is actually possible to calculate optimum three dimensional transonic wing shapes in a few hours, accounting for viscous effects with the flow modeled by the Reynolds averaged Navier Stokes (RANS) equations. By enforcing constraints on the thickness and span-load distribution one can make sure that there is no penalty in structure weight or fuel volume. Larger scale shape changes such as planform variations can also be accommodated.[7] It then becomes necessary to include a structural weight model to enable a proper compromise between minimum drag and low structure weight to be determined.

Aerodynamic shape optimization has been successfully performed for a variety of complex configurations using multi-block structured meshes.[8,9] Meshes of this type can be relatively easily deformed to accommodate shape variations required in the redesign. However, it is both extremely time-consuming and expensive in human costs to generate such meshes. Consequently we believe it is essential to develop shape optimization methods which use unstructured meshes for the flow simulation.

Typically, in gradient-based optimization techniques, a control function to be optimized (the wing shape, for example) is parameterized with a set of design variables and a suitable cost function to be minimized is defined. For aerodynamic problems, the cost function is typically lift, drag or a specified target pressure distribution. Then, a constraint, the governing equations can be introduced in order to express the dependence between the cost function and the control function. The sensitivity derivatives of the cost function with respect to the design variables are calculated in order to get a direction of improvement. Finally, a step is taken in this direction and the procedure is repeated until convergence is achieved. Finding a fast and accurate way of calculating the necessary gradient information is essential to developing an effective design method since this can be the most time consuming portion of the design process. This is particularly true in problems which involve a very large number of design variables as is the case in a typical three dimensional shape optimization.

The control theory approach[20–22] has dramatic computational cost advantages over the finite-difference method of calculating gradients. With this approach the necessary gradients are obtained through the solution of an adjoint system of equations of the governing equations of interest. The adjoint method is extremely efficient since the computational expense incurred in the calculation of the complete gradient is effectively independent of the number of design variables.

In this study, a continuous adjoint formulation has been used to derive the adjoint system of equations. Accordingly, the adjoint equations are derived directly from the governing equations and then discretized. This approach has the advantage over the discrete adjoint formulation in that the resulting adjoint equations are independent of the form of discretized flow equations. The adjoint system of equations have a similar form to the governing equations of the flow and hence the numerical methods developed for the flow

*Professor, Stanford University
†Professor, Princeton University

Copyright © 2003 by Antony Jameson. Published by the American Institute of Aeronautics and Astronautics, Inc. with permission.

equations[10,12,13] can be reused for the adjoint equations.

The gradient is derived solely from the adjoint solution and the surface displacement, independent of the mesh modification. This is crucial for unstructured meshes. If the gradient depends on the form of the mesh modification, then the field integral in the gradient calculation has to be recomputed for mesh modifications corresponding to each design variable. This would be prohibitively expensive if the geometry is treated as a free surface defined by the mesh points. Consequently in order to reduce the computational cost with this approach,[14–16] the number of design variables would have to be reduced by parameterizing the geometry. However, this reduced set of design variables could not recover all possible shape variations.

A steepest descent method is finally used to improve the initial design. In order to guarantee that the shape variations remain sufficiently smooth the gradients are redefined so that they correspond to an inner product in a Sobolev space. This is accomplished by an implicit smoothing procedure which also acts as an effective pre-conditioner, with the result that the number of design steps needed to reach an optimum is quite small, of the order of 20-50.

The General Formulation of the Adjoint Approach to Optimal Design

For flow about an airfoil, or wing, the aerodynamic properties which define the cost function are functions of the flow-field variables, w, and the physical location of the boundary, which may be represented by the function, $\mathcal{F}$, say. Then

$$I = I(w, \mathcal{F}),$$

and a change in $\mathcal{F}$ results in a change

$$\delta I = \frac{\partial I^T}{\partial w}\delta w + \frac{\partial I^T}{\partial \mathcal{F}}\delta \mathcal{F}, \tag{1}$$

in the cost function. Using control theory, the governing equations of the flow field are introduced as a constraint in such a way that the final expression for the gradient does not require re-evaluation of the flow-field. In order to achieve this, δw must be eliminated from equation 1. Suppose that the governing equation R which expresses the dependence of w and $\mathcal{F}$ within the flow field domain D can be written as

$$R(w, \mathcal{F}) = 0 \tag{2}$$

Then δw is determined from the equation

$$\delta R = \left[\frac{\partial R}{\partial w}\right]\delta w + \left[\frac{\partial R}{\partial \mathcal{F}}\right]\delta \mathcal{F} = 0 \tag{3}$$

Next, introducing a Lagrange Multiplier ψ, we have

$$\delta I = \frac{\partial I^T}{\partial w}\delta w + \frac{\partial I^T}{\partial \mathcal{F}}\delta \mathcal{F} - \psi^T\left(\left[\frac{\partial R}{\partial w}\right]\delta w + \left[\frac{\partial R}{\partial \mathcal{F}}\right]\delta \mathcal{F}\right)$$

$$\delta I = \left(\frac{\partial I^T}{\partial w} - \psi^T\left[\frac{\partial R}{\partial w}\right]\partial w\right)\delta w + \left(\frac{\partial I^T}{\partial \mathcal{F}} - \psi^T\left[\frac{\partial R}{\partial \mathcal{F}}\right]\delta \mathcal{F}\right)$$

Choosing ψ to satisfy the adjoint equation

$$\left[\frac{\partial R}{\partial w}\right]^T \psi = \frac{\partial I}{\partial w} \tag{4}$$

the first term is eliminated and we find that

$$\delta I = \mathcal{G}\delta \mathcal{F} \tag{5}$$

where

$$\mathcal{G} = \frac{\partial I^T}{\partial \mathcal{F}} - \psi^T\left[\frac{\partial R}{\partial \mathcal{F}}\right] \tag{6}$$

This process allows for elimination of the terms that depend on the flow solution with the result that the gradient with respect with an arbitrary number of design variables can be determined without the need for additional flow field evaluations.

After taking a step in the negative gradient direction, the gradient is recalculated and the process repeated to follow the path of steepest descent until a minimum is reached. In order to avoid violating constraints, such as the minimum acceptable wing thickness, the gradient can be projected into an allowable subspace within which the constraints are satisfied. In this way one can devise procedures which must necessarily converge at least to a local minimum and which can be accelerated by the use of more sophisticated descent methods such as conjugate gradient or quasi-Newton algorithms. There is a possibility of more than one local minimum, but in any case this method will lead to an improvement over the original design.

Design using the Euler Equations

The application of control theory to aerodynamic design problems is illustrated in this section for the case of three-dimensional wing design using the compressible Euler equations as the mathematical model. It proves convenient to denote the Cartesian coordinates and velocity components by x_1, x_2, x_3 and u_1, u_2, u_3, and to use the convention that summation over $i = 1$ to 3 is implied by a repeated index i. Then, the three-dimensional Euler equations may be written as

$$\frac{\partial w}{\partial t} + \frac{\partial f_i}{\partial x_i} = 0 \quad \text{in } D, \tag{7}$$

where

$$w = \begin{Bmatrix} \rho \\ \rho u_1 \\ \rho u_2 \\ \rho u_3 \\ \rho E \end{Bmatrix}, \quad f_i = \begin{Bmatrix} \rho u_i \\ \rho u_i u_1 + p\delta_{i1} \\ \rho u_i u_2 + p\delta_{i2} \\ \rho u_i u_3 + p\delta_{i3} \\ \rho u_i H \end{Bmatrix} \tag{8}$$

and δ_{ij} is the Kronecker delta function. Also,

$$p = (\gamma - 1)\,\rho\left\{E - \frac{1}{2}\left(u_i^2\right)\right\}, \tag{9}$$

and

$$\rho H = \rho E + p \tag{10}$$

where γ is the ratio of the specific heats.

Consider a transformation to coordinates ξ_1, ξ_2, ξ_3 where

$$K_{ij} = \left[\frac{\partial x_i}{\partial \xi_j}\right], \quad J = \det(K), \quad K_{ij}^{-1} = \left[\frac{\partial \xi_i}{\partial x_j}\right],$$

and

$$S = JK^{-1}.$$

The elements of S are the cofactors of K, and in a finite volume discretization they are just the face areas of the computational cells projected in the x_1, x_2, and x_3 directions. Using the permutation tensor ϵ_{ijk} we can express the elements of S as

$$S_{ij} = \frac{1}{2}\epsilon_{jpq}\epsilon_{irs}\frac{\partial x_p}{\partial \xi_r}\frac{\partial x_q}{\partial \xi_s}. \tag{11}$$

Then

$$\begin{aligned}\frac{\partial}{\partial \xi_i}S_{ij} &= \frac{1}{2}\epsilon_{jpq}\epsilon_{irs}\left(\frac{\partial^2 x_p}{\partial \xi_r \partial \xi_i}\frac{\partial x_q}{\partial \xi_s} + \frac{\partial x_p}{\partial \xi_r}\frac{\partial^2 x_q}{\partial \xi_s \partial \xi_i}\right)\\ &= 0.\end{aligned} \tag{12}$$

Now, multiplying equation(7) by J and applying the chain rule,

$$J\frac{\partial w}{\partial t} + R(w) = 0 \tag{13}$$

where

$$R(w) = S_{ij}\frac{\partial f_j}{\partial \xi_i} = \frac{\partial}{\partial \xi_i}(S_{ij}f_j), \tag{14}$$

using (12). We can write the transformed fluxes in terms of the scaled contravariant velocity components

$$U_i = S_{ij}u_j$$

as

$$F_i = S_{ij}f_j = \begin{bmatrix} \rho U_i \\ \rho U_i u_1 + S_{i1}p \\ \rho U_i u_2 + S_{i2}p \\ \rho U_i u_3 + S_{i3}p \\ \rho U_i H \end{bmatrix}.$$

Assume now that the new computational coordinate system conforms to the wing in such a way that the wing surface B_W is represented by $\xi_2 = 0$. Then the flow is determined as the steady state solution of equation (13) subject to the flow tangency condition

$$U_2 = 0 \quad \text{on } B_W. \tag{15}$$

At the far field boundary B_F, conditions are specified for incoming waves, as in the two-dimensional case, while outgoing waves are determined by the solution.

The weak form of the Euler equations for steady flow can be written as

$$\int_{\mathcal{D}} \frac{\partial \phi^T}{\partial \xi_i}F_i d\mathcal{D} = \int_{\mathcal{B}} n_i \phi^T F_i d\mathcal{B}, \tag{16}$$

where the test vector ϕ is an arbitrary differentiable function and n_i is the outward normal at the boundary. If a differentiable solution w is obtained to this equation, it can be integrated by parts to give

$$\int_{\mathcal{D}} \phi^T \frac{\partial F_i}{\partial \xi_i} d\mathcal{D} = 0$$

and since this is true for any ϕ, the differential form can be recovered. If the solution is discontinuous (16) may be integrated by parts separately on either side of the discontinuity to recover the shock jump conditions.

Suppose now that it is desired to control the surface pressure by varying the wing shape. For this purpose, it is convenient to retain a fixed computational domain. Then variations in the shape result in corresponding variations in the mapping derivatives defined by K. As an example, consider the case of an inverse problem, where we introduce the cost function

$$I = \frac{1}{2}\iint_{B_W}(p - p_d)^2\, d\xi_1 d\xi_3,$$

where p_d is the desired pressure. The design problem is now treated as a control problem where the control function is the wing shape, which is to be chosen to minimize I subject to the constraints defined by the flow equations (13). A variation in the shape will cause a variation δp in the pressure and consequently a variation in the cost function

$$\delta I = \iint_{B_W}(p - p_d)\,\delta p \;\; d\xi_1 d\xi_3 + \frac{1}{2}\int_{\mathcal{B}}(p - p_t)^2 d\delta S \tag{17}$$

where typically the second term is negligible and can be dropped.

Since p depends on w through the equation of state (9–10), the variation δp can be determined from the variation δw. Define the Jacobian matrices

$$A_i = \frac{\partial f_i}{\partial w}, \quad C_i = S_{ij}A_j. \tag{18}$$

The weak form of the equation for δw in the steady state becomes

$$\int_{\mathcal{D}} \frac{\partial \phi^T}{\partial \xi_i}\delta F_i d\mathcal{D} = \int_{\mathcal{B}}(n_i \phi^T \delta F_i) d\mathcal{B},$$

where

$$\delta F_i = C_i \delta w + \delta S_{ij} f_j,$$

which should hold for any differential test function ϕ. This equation may be added to the variation in the cost function, which may now be written as

$$\begin{aligned}\delta I = &\iint_{B_W} (p - p_d)\, \delta p \;\; d\xi_1 d\xi_3 \\ &- \int_{\mathcal{D}} \left(\frac{\partial \phi^T}{\partial \xi_i} \delta F_i \right) d\mathcal{D} \\ &+ \int_{\mathcal{B}} \left(n_i \phi^T \delta F_i \right) d\mathcal{B}. \end{aligned} \tag{19}$$

On the wing surface B_W, $n_1 = n_3 = 0$. Thus, it follows from equation (15) that

$$\delta F_2 = \begin{bmatrix} 0 \\ S_{21}\delta p \\ S_{22}\delta p \\ S_{23}\delta p \\ 0 \end{bmatrix} + \begin{bmatrix} 0 \\ \delta S_{21} p \\ \delta S_{22} p \\ \delta S_{23} p \\ 0 \end{bmatrix}. \tag{20}$$

Since the weak equation for δw should hold for an arbitrary choice of the test vector ϕ, we are free to choose ϕ to simplify the resulting expressions. Therefore we set $\phi = \psi$, where the co-state vector ψ is the solution of the adjoint equation

$$\frac{\partial \psi}{\partial t} - C_i^T \frac{\partial \psi}{\partial \xi_i} = 0 \quad \text{in } D. \tag{21}$$

At the outer boundary incoming characteristics for ψ correspond to outgoing characteristics for δw. Consequently one can choose boundary conditions for ψ such that

$$n_i \psi^T C_i \delta w = 0.$$

Then, if the coordinate transformation is such that δS is negligible in the far field, the only remaining boundary term is

$$-\iint_{B_W} \psi^T \delta F_2 \; d\xi_1 d\xi_3.$$

Thus, by letting ψ satisfy the boundary condition,

$$S_{21}\psi_2 + S_{22}\psi_3 + S_{23}\psi_4 = (p - p_d) \quad \text{on } B_W, \tag{22}$$

we find finally that

$$\begin{aligned}\delta I \quad &= - \int_{\mathcal{D}} \frac{\partial \psi^T}{\partial \xi_i} \delta S_{ij} f_j d\mathcal{D} \\ &- \iint_{B_W} (\delta S_{21}\psi_2 + \delta S_{22}\psi_3 + \delta S_{23}\psi_4)\, p \, d\xi_1 d\xi_3. \end{aligned} \tag{23}$$

Here the expression for the cost variation depends on the mesh variations throughout the domain which appear in the field integral. However, the true gradient for a shape variation should not depend on the way in which the mesh is deformed, but only on the true flow solution. In the next section, we show how the field integral can be eliminated to produce a reduced gradient formula which depends only on the boundary movement.

Reduced Gradient Formulations

Continuous adjoint formulations have generally used a form of the gradient that depends on the manner in which the mesh is modified for perturbations in each design variable. To represent all possible shapes the control surface should be regarded as a free surface. If the surface mesh points are used to define the surface, this leaves the designer with a thousands of design variables. On an unstructured mesh evaluating the gradient by perturbing each design variable in turn, would be prohibitively expensive because of the need to determine corresponding perturbations of the entire mesh. This would inhibit the use of this design tool in any meaningful design process.

In order to avoid this difficulty an alternate formulation to the gradient calculation is followed in this study. This idea was developed by Jameson and Sangho Kim[24] and was validated for two and three dimensional problems with structured grids. However, as it is possible to devise mesh modification routines that are computationally cheap on structured grids, the major benefit of this alternate gradient formulation is for general three dimensional unstructured grids. To complete the formulation of the control theory approach to shape optimization, the gradient formulations are outlined next. The formulation for the reduced gradients in the continuous limit is presented in the context of transformation between the physical domain and the computational domain, and is easily extended to unstructured grid methods where these transformations are not explicitly used.

The evaluation of the field integral in equation (23) requires the evaluation of the metric variations δS_{ij} throughout the domain. However, the true gradient should not depend on the way the mesh is modified.

Consider the case of a mesh variation with a fixed boundary. Then,

$$\delta I = 0$$

but there is a variation in the transformed flux,

$$\delta F_i = C_i \delta w + \delta S_{ij} f_j.$$

Here the true solution is unchanged. Thus, the variation δw is due to the mesh movement δx at fixed boundary configuration. Therefore

$$\delta w = \nabla w \cdot \delta x = \frac{\partial w}{\partial x_j} \delta x_j \; (= \delta w^*)$$

and since

$$\frac{\partial}{\partial \xi_i} \delta F_i = 0,$$

it follows that

$$\frac{\partial}{\partial \xi_i} \left(\delta S_{ij} f_j \right) = - \frac{\partial}{\partial \xi_i} \left(C_i \delta w^* \right). \tag{24}$$

It is verified in reference[24] that this relation holds in the general case with boundary movement. Now

$$\begin{aligned}\int_{\mathcal{D}} \psi^T \delta R d\mathcal{D} &= \int_{\mathcal{D}} \psi^T \frac{\partial}{\partial \xi_i} C_i \left(\delta w - \delta w^*\right) d\mathcal{D} \\ &= \int_{\mathcal{B}} \psi^T C_i \left(\delta w - \delta w^*\right) d\mathcal{B} \\ &- \int_{\mathcal{D}} \frac{\partial \psi^T}{\partial \xi_i} C_i \left(\delta w - \delta w^*\right) d\mathcal{D}. \quad (25)\end{aligned}$$

Here on the wall boundary

$$C_2 \delta w = \delta F_2 - \delta S_{2j} f_j. \quad (26)$$

Thus, by choosing ψ to satisfy the adjoint equation and the adjoint boundary condition, we have finally the cost variation that is reduced to a boundary integral

$$\begin{aligned}\delta I &= \int_{\mathcal{B}_{\mathcal{W}}} \psi^T \left(\delta S_{2j} f_j + C_2 \delta w^*\right) d\xi_1 d\xi_3 \\ &- \int\int_{B_W} (\delta S_{21} \psi_2 + \delta S_{22} \psi_3 + \ \delta S_{23} \psi_4)\, p\, d\xi_1 d\xi_3 \quad (27)\end{aligned}$$

In this reduced formulation the cost variation depends only on the boundary shape variations with the result that the gradient can be evaluated without any knowledge of the mesh deformation.

The need for a Sobolev inner product in the definition of the gradient

Another key issue for successful implementation of the continuous adjoint method is the choice of an appropriate inner product for the definition of the gradient. It turns out that there is an enormous benefit from the use of a modified Sobolev gradient, which enables the generation of a sequence of smooth shapes. This can be illustrated by considering the simplest case of a problem in calculus of variations.

Choose $y(x)$ to minimize

$$I = \int_a^b F(y, y^{'}) dx$$

with fixed end points $y(a)$ and $y(b)$. Under a variation $\delta y(x)$,

$$\begin{aligned}\delta I &= \int_a^b \left(\frac{\partial F}{\partial y}\delta y + \frac{\partial F}{\partial y^{'}}\delta y^{'}\right) dx \\ &= \int_a^b \left(\frac{\partial F}{\partial y} - \frac{d}{dx}\frac{\partial F}{\partial y^{'}}\right) \delta y dx\end{aligned}$$

Thus defining the gradient as

$$g = \frac{\partial F}{\partial y} - \frac{d}{dx}\frac{\partial F}{\partial y^{'}}$$

and the inner product as

$$(u, v) = \int_a^b uv dx$$

we find that

$$\delta I = (g, \delta y)$$

Then if we set

$$\delta y = -\lambda g, \qquad \lambda > 0$$

we obtain a improvement

$$\delta I = -\lambda (g, g) \leq 0$$

unless $g = 0$, the necessary condition for a minimum. Note that g is a function of $y, y^{'}, y^{''}$,

$$g = g(y, y^{'}, y^{''})$$

In the case of the Brachistrone problem, for example

$$g = -\frac{1 + y^{'2} + 2yy^{''}}{2\left(y(1 + y^{'2})\right)^{3/2}}$$

Now each step

$$y^{n+1} = y^n - \lambda^n g^n$$

reduces the smoothness of y by two classes. Thus the computed trajectory becomes less and less smooth, leading to instability.

In order to prevent this we can introduce a modified Sobolev inner product[23]

$$\langle u, v \rangle = \int (uv + \epsilon u^{'} v^{'}) dx$$

where ϵ is a parameter that controls the weight of the derivatives. If we define a gradient $\overline{g}$ such that

$$\delta I = \langle \overline{g}, \delta y \rangle$$

Then we have

$$\begin{aligned}\delta I &= \int (\overline{g}\delta y + \epsilon \overline{g}^{'} \delta y^{'}) dx \\ &= \int (\overline{g} - \frac{\partial}{\partial x}\epsilon \frac{\partial \overline{g}}{\partial x}) \delta y dx \\ &= (g, \delta y)\end{aligned}$$

where

$$\overline{g} - \frac{\partial}{\partial x}\epsilon \frac{\partial \overline{g}}{\partial x} = g$$

and $\overline{g} = 0$at the end points. Thus $\overline{g}$ is obtained from g by a smoothing equation.

Now the step

$$y^{n+1} = y^n - \lambda^n \overline{g}^n$$

gives an improvement

$$\delta I = -\lambda^n \langle \overline{g}^n, \overline{g}^n \rangle$$

but y^{n+1} has the same smoothness as y^n, resulting in a stable process.

In applying control theory for aerodynamic shape optimization, the use of a Sobolev gradient is equally important for the preservation of the smoothness class of the redesigned surface and we have employed it to obtain all the results in this study.

Imposing Thickness Constraints on Unstructured Meshes

In order to perform meaningful drag reduction computations, it is necessary to ensure that constraints such as the thickness of the wing are satisfied during the design process. On an arbitrary unstructured mesh there appears to be no straightforward way to impose thickness constraints. In our approach we introduce cutting-planes at various span-wise locations along the wing and tranform the airfoil sections to shallow bumps by a square root mapping. Then we interpolate the gradients from the nodes on the surface to the airfoil sections on the cutting-planes, and impose the thickness constraints on the mapped sections. The displacements of the points on the surface of the CFD mesh are obtained by interpolation from the mapped airfoil sections, and transformed back to the physical domain by a reverse mapping. These surface displacements are finally used as inputs to a mesh deformation algorithm.

Mesh Deformation

The modifications to the shape of the boundary are transferred to the volume mesh using the spring method. This approach has been found to be adequate for the computations performed in this study.

The spring method can be mathematically conceptualized as solving the following equation

$$\frac{\partial \Delta x_i}{\partial t} + \sum_{j=1}^{N} K_{ij}(\Delta x_i - \Delta x_j) = 0$$

where the K_{ij} is the stiffness of the edge connecting node i to node j and its value is inversely proportional to the length of this edge, Δx_i is the displacement of node i and Δx_j is the displacement of node j, the opposite end of the edge. The position of static equilibrium of the mesh is computed using a Jacobi iteration with known initial values for the surface displacements.

Overview of the Design Process

A flow-chart describing the overall design process is shown in figure 3.

Numerical Discretization and Convergence Acceleration Techniques for the Flow and Adjoint Equations

The numerical algorithms and convergence acceleration techniques used in this study to obtain steady state solutions for the Euler equations, are based on a finite element approximation, initially reported in Jameson, Baker and Weatherill.[11] The method is described here for completeness. Due to the remarkable similarity between the adjoint system and the flow equations, essentially the same numerical schemes can be reused to obtain the solution to the adjoint system.

The finite element approximation can be obtained by directly approximating the integral equations for the balance of mass, momentum and energy in polyhedral control volumes. Each of these is formed by the union of the tetrahedra meeting at a common vertex (figure 1). It turns out that the flux balance can be broken down into contributions of fluxes through faces in a very elegant way (figure 2). This decomposition reduces the evaluation of the Euler equations to a single main loop over the faces. It is shown in Jameson, Baker and Weatherill[11] that the same discretization can also be devised from the weak form of the equations, using linear trial solutions and test functions. Thus it is essentially equivalent to a Galerkin method.

Shock waves are captured with the assistance of added artificial dissipation. These shock capturing schemes are derived from general class of schemes that maintain the positivity of the co-efficients, thereby preventing maximas from increasing and minimas from decreasing. Steady state solutions are obtained by integrating the time dependent equations with a multistage time stepping scheme. Convergence is accelerated by the use of locally varying time steps, residual averaging and enthalpy damping. Multigrid techniques are also used to further improve convergence to the steady state.

Computational Methodology and Finite Element Approximation

The Euler equations in integral form can be written as

$$\frac{d}{dt}\int_V w dV + \int_S F \cdot dS = 0 \tag{28}$$

Equation(28) can be approximated on a tetrahedral mesh by first writing the flux balance for each tetrahedron assuming the fluxes (F) to vary linearly over each face. Then at any given mesh point one considers the rate of change of w for a control volume consisting of the union of the tetrahedra meeting at a common vertex. This gives

$$\frac{d}{dt}\left(\sum_k V_k w\right) + \sum_k R_k = 0. \tag{29}$$

where V_k is the volume of the k^{th} tetrahedron meeting at a given mesh point and R_k is the flux of that tetrahedron.

When the flux balances of the neighboring tetrahedra are summed, all contributions across interior faces cancel. Referring to figure 2, which illustrates a portion of a three dimensional mesh, it may be seen that with a tetrahedral mesh, each face is a common external boundary of exactly two control volumes. Therefore each internal face can be associated with a set of 5 mesh points consisting of its corners 1,2 and 3, and the vertices 4 and 5 of the two control volumes on either side of the common face. It is now possible to generate the approximation in equation(29), by pre-setting the flux balance at each mesh point to zero, and then performing a single loop over the faces. For each face, one first calculates the fluxes of mass, momentum and energy across each face, and then one assigns these contributions of the vertices 4 and 5 with positive and negative signs respectively. Since every contribution is transferred from one control volume into another, all quantities are perfectly conserves. Mesh points on the inner and outer boundaries lie on the surface of their own control volumes, and the accumulation of the flux balance in these volumes has to be correspondingly modified. At a solid surface it is also necessary to enforce the boundary condition that there is no convective flux through the faces contained in the surface.

While the original formulation of this method used a face based loop to accumulate the fluxes, the first author later modified the loops to go through the edges in the mesh as they were typically smaller in number than the faces. The above arguments for flux accumulation extend easily to edge-based schemes and it is this approach that has been used in the current study.

Dissipation

A simple way to introduce dissipation is to add a term generated from the difference between the value at a given node and its nearest neighbors. That is, at node 0, we add a term

$$D_o = \sum_k \epsilon_{ko}^{(1)}(w_k - w_o) \tag{30}$$

where the sum is over the nearest neighbors. This contribution is balanced by a corresponding contribution at node k, with the result that the scheme remains conservative. The coefficients $\epsilon_{ko}^{(1)}$ may incorporate metric information depending on local cell volumes and face areas, and can also be adapted to gradients of the solution. As equation (30) is only first-order accurate (unless the coefficients are proportional to the mesh spacing), a more accurate scheme is obtained by recycling the edge differencing procedure. After setting

$$E_o = \sum_k (w_k - w_o) \tag{31}$$

at every mesh point, one then sets

$$D_o = -\sum_k \epsilon_{ok}^{(2)}(E_k - E_o) \tag{32}$$

An effective scheme is produced by blending equation (30) and (32), and adapting $\epsilon_{ko}^{(1)}$ to the local pressure gradient. This scheme has been found to have good shock capturing properties and the required sums can be efficiently assembled by loops over the edges.

Other shock capturing schemes that satisfy the LED property have also been implemented, and have been found to work equally efficiently. However, due to the robust nature of the simple scalar dissipation model described above, we have used it for all the computations in this study.

Integration to Steady State and Convergence Acceleration Techniques

The resulting spatial discretizations yield a set of coupled ordinary differential equations that can be integrated in time to obtain steady state solutions of the Euler equations. To maximize the allowable time step, the same multistage schemes that have proven to be efficient in rectilinear meshes[17] have been used on unstructured meshes. These schemes bear close resemblance to Runge-Kutta schemes with modifications to the evaluation of the dissipation terms that enlarge the stability limit of the scheme along the imaginary axis, thereby allowing convective waves to be resolved.

Convergence to steady state is accelerated by using a variable time step close to the stability limit of each mesh point. The scheme is accelerated further by the introduction of residual averaging[18] and multigrid procedure.[19] In this study, the coarser grids are either obtained through an independent mesh generator or through an edge-collapsing algorithm. In either approach, transfer coefficients between the various meshes are accumulated in a pre-processing step and recomputed when the meshes are deformed.

Modifications to the Numerical Method to Treat the Adjoint Equations

In order to adapt the numerical scheme to treat the adjoint equations three main modifications are required.

First, because the adjoint equation appears in a non-conservative quasi-linear form, the convective terms have to be calculated in a different manner. The derivatives $\frac{\partial \psi}{\partial x_i}$ are calculated by applying the Gauss theorem to the polyhedral control volume consisting of the tetrahedrons that surround each node. Thus the formula

$$\frac{\partial \psi}{\partial x_i} = \frac{1}{V}\int_S \psi dS_{x_i} \tag{33}$$

is replaced by its discrete analog, and the contributions are accumulated by edge and face loops in the same manner as the flux balance of equation (28). The

transposed Jacobian matrices are simplified by using a transformation to the symmetrizing variables. Thus the Jacobian for flux in the x direction is expressed as

$$A = M\hat{A}M^{-1}, A^T = M^{-1}\hat{A}M^T$$

where

$$M = \begin{pmatrix} \frac{\rho}{c} & 0 & 0 & 0 & -\frac{1}{c^2} \\ \frac{\rho u}{c} & \rho & 0 & 0 & -\frac{u}{c^2} \\ \frac{\rho v}{c} & 0 & \rho & 0 & -\frac{v}{c^2} \\ \frac{\rho w}{c} & 0 & 0 & \rho & -\frac{w}{c^2} \\ \frac{\rho H}{c} & \rho u & \rho v & \rho w & -\frac{q^2}{2c^2} \end{pmatrix} \quad (34)$$

and

$$\hat{A} = \begin{pmatrix} Q & S_x c & S_y c & S_y c & 0 \\ S_x c & Q & 0 & 0 & 0 \\ S_y c & 0 & Q & 0 & 0 \\ S_z c & 0 & 0 & Q & 0 \\ 0 & 0 & 0 & 0 & Q \end{pmatrix} \quad (35)$$

Second, the direction of time integration to a steady state is reversed because the directions of wave propagation are reversed. Third, while the artificial diffusion terms are calculated by the same subroutines that are used for the flow solution, they are subtracted instead of added to the convective terms to give a downwind instead of an upwind bias. Because of the reversed sign of the time derivatives the diffusive terms in the time dependent equation correspond to the diffusion equation with the proper sign.

Results

The adjoint method described in the previous sections has been applied to two and three dimensional problems with the flow modeled by the Euler equations. Both drag reduction and inverse design problems were used to validate the design procedure and the gradient formulations. The method was then used to redesign the shape of the wing of a transonic business jet, where the complete aircraft configuration was modeled. A flow-chart describing the overall design process is shown in figure 3.

Airfoil Design

The unstructured adjoint technology was initially validated for two-dimensional inverse design and drag minimization problems. Figures 4 and 5, show the result of drag minimization for the RAE 2822 airfoil in transonic flow ($M_\infty = 0.75$). The lift was constrained to be 0.6 and the angle of attack was perturbed to maintain the lift. The final geometry is shock-free and the drag was reduced by 36 drag counts. Figures 4 and 6 show the result of an inverse design for the RAE 2822 airfoil. Here the target pressure distribution was a shock-free profile obtained from the drag minimization exercise. As can be seen from these pictures, the final pressure profile almost exactly matches the target pressure distribution.

Wing Design

The design methodology was then applied to wing shapes in transonic flow. Inverse design computations were performed to validate the design process and the gradient calculations. Figure 8 shows the result of an inverse design calculation, where the initial geometry was a wing with NACA 0012 sections and the target pressure distribution was the pressure distribution over the Onera M6 wing. Figures 9, 10, 11, 12, show the target and computed pressure distribution at 4 span-wise sections. It can be seen from these plots the target pressure distribution is almost perfectly recovered in 50 design cycles. The results from this test case show that the design process is capable of recovering pressure distributions that are significantly different from the initial distribution and can also capture shocks and other discontinuities in the target pressure distribution.

Another test case for the inverse design problem used the wing from an airplane (SHARK[25]) that was designed for the Reno Air Races. The initial and target pressure distributions are shown the figure 13. As can be seen from these plots, the initial pressure distribution has a weak shock in the outboard sections of the wing. The target pressure distribution is shock-free. The computed (after 50 design cycles) and target pressure distributions along three sections of the wing are shown in figures 14, 15, 16. Again the design process captures the target pressure with good accuracy in about 50 design cycles.

Shape Optimization of a Transonic Business Jet

The design method has finally been applied to complete aircraft configurations. As a representative example we show the redesigns of a transonic business jet to improve its lift to drag ratio during cruise. As shown in figures 17, 18, 19, 20, the outboard sections of the wing have a strong shock while flying at cruise conditions ($M_\infty = 0.80$, $\alpha = 2^o$). The results of a drag minimization that aims to remove the shocks on the wing are shown in figures 21, 22, 23, 24. The drag has been reduced from 235 counts to 215 counts in about 8 design cycles. The lift was constrained at 0.4 by perturbing the angle of attack. Further, the original thickness of the wing was maintained during the design process ensuring that fuel volume and structural integrity will be maintained by the redesigned shape. The entire design process typically takes about 4 hours on a 1.7 Ghz Athlon processor with 1 Gb of memory. Parallel implementation of the design procedure has also been developed that further reduces the computational cost of this design process.

Conclusions

The use of gradient formulations that depend only of the surface mesh allows adjoint based methods to

be used for unstructured grids in a computationally efficient manner. Hence, it is now possible to devise a completely automated shape optimization procedure for complete aircraft configurations. Exploiting the flexibility of unstructured grids, it is now possible to tackle wing section and planform optimization, engine-integration and empennage design with an integrated computational procedure. Hence, we believe that this approach holds great promise for airplane design.

Ongoing and Future Directions of Research

Our results provide a verification that an unstructured adjoint method is both computationally feasible, and can satisfy the typical constraints encountered in aerodynamic design. We plan to leverage this ability to provide an engineering tool for airplane designers by using a CAD interface to perform the shape modification. We believe that this capability will provide the designer with a consistent CAD definition of the final redesigned shape that can be used for either structural analysis or for manufacturing purposes. Using this tool we plan eventually to include all the major components in the design, such as pylon, winglet, nacelle, fin and tail shapes, along with the intersections of the various components. We have already performed flow simulations of a variety of airplane configurations in transonic and supersonic flight (figures 25, 26, 27 and 28), and plan to show redesigns of some of these configurations during the Aerospace Sciences Meeting at Reno in 2004.

References

[1]Jameson A., Optimum Aerodynamic Design Using Control Theory, *Computational Fluid Dynamics Review*, 1995, pp. 495-528.

[2]A. Jameson and Luigi Martinelli, Aerodynamic Shape Optimization Techniques Based on Control Theory, *CIME (International Mathematical Summer Center)*, Martina Fran-ca, Italy, June 1999.

[3]A. Jameson, J. Alonso, J. Reuther, L. Martinelli,J. Vassberg, Aerodynamic Shape Optimization Techniques Based on Control Theory, *AIAA paper 98-2538*, 29th AIAA Fluid Dynamics Conference, Alburquerque, June 1998.

[4]Siva K. Nadarajah and Antony Jameson, Optimal Control of Unsteady Flows using a Time Accurate Method, *AIAA-2002-5436, 9th AIAA/ISSMO Symposium on Multidisciplinary Analysis and Optimization Conference*, September 4-6, 2002, Atlanta, GA.

[5]Jameson A., Optimum Aerodynamic Design via Boundary Control, *RIAC Technical Report 94.17, Princeton University Report MAE 1996, Proceedings of AGARD FDP/Von Karman Institute Special Course on "Optimum Design Methods in Aerodynamics"*, Brussels, April 1994, pp. 3.1-3.33.

[6]Jameson A.,L. Martinelli,N. Pierce, Optimum Aerodynamic Design using the Navier Stokes Equation, *Theoretical and Computational Fluid Dynamics*, Vol. 10, 1998, pp213-237.

[7]Kasidit Leoviriyakit and A. Jameson, Aerodynamic Shape Optimization of Wings including Planform Variations, *AIAA Paper 2003-0210*, Reno, NV, January 6-9, 2003.

[8]Reuther, J. J., Alonso, J. J., Jameson, A., Rimlinger, M. J., Saunders, D., Constrained Multipoint Aerodynamic Shape Optimization Using an Adjoint Formulation and Parallel Computers: Part I,II *AIAA Paper 97-0103* 35^{th} Aerospace Sciences Meeting, Reno, Nevada, *Journal of Aircraft*, vol. 36, no., 1, pp. 51-60,61-74, January-February 1999.

[9]S. Cliff, J. Reuther, D. Sanders and R. Hicks, Single and Multipoint Aerodynamic Shape Optimization of High Speed Civil Transport, *Journal of Aircraft*, Vol. 38, No. 6, pp. 997-1005, Nov-Dec. 2001.

[10]A. Jameson, W. Schmidt and E. Turkel, Numerical Solution of the Euler equations by finite volume methods using Runger-Kutta time stepping schemes, *AIAA Paper 81-1259*, June, 1981.

[11]A. Jameson, T.J. Baker and N.P. Weatherill, Calculation of Inviscid Transonic Flow over a Complete Aircraft *AIAA Paper 86-0103*, 24^{th} AIAA Aerospace Sciences Meeting, Reno, January, 1986.

[12]A. Jameson and T.J. Baker, Improvements to the Aircraft Euler Method, *AIAA Paper 87-0353*, 25^{th} AIAA Aerospace Sciences Meeting, Reno, January, 1987.

[13]T.J. Barth, Apects of unstructured grids and finite volume solvers for the Euler and Navier-Stokes equations, *AIAA Paper 91-0237*, 29^{th} AIAA Aerospace Sciences Meeting, Reno, January, 1994.

[14]J. Elliot and J. Peraire, Aerodynamic design using unstructured meshes, *AIAA Paper 96-1941*, 33^{rd} AIAA Aerospace Sciences Meeting, Reno January, 1996.

[15]K. Anderson and V. Venkatakrishnan, Aerodynamic Design Optimization on Unstructured grids using a continuous adjoint formulation, *AIAA Paper 97-0643*, 34^{th} AIAA Aerospace Sciences Meeting, Reno, January, 1997.

[16]S. E. Cliff, S.D. Thomas, T. J. Baker, A. Jameson and R. M. Hicks, Aerodynamic Shape optimization using unstructured grid method, *AIAA Paper 02-5550*, 9^{th} AIAA Symposium on Multidisciplinary Analysis and Optimization, Atlanta, September, 2002.

[17]A. Jameson, Transonic Flow Calculations, *Princeton University, MAE Report No. 1651.*

[18]T. H. Pulliam and J. L. Steger, Implicit Finite Difference Simulations of three dimensional Compressible Flow, *AIAA Journal* Vol. 18, 1980, pp. 159-167.

[19]Jameson A., Mavriplis D J and Martinelli L, Multigrid Solution of the Navier-Stokes Equations on Triangular Meshes, *ICASE Report 89-11*, *AIAA Paper 89-0283*, AIAA 27th Aerospace Sciences Meeting, Reno, January, 1989.

[20]O. Pironneau, Optimal Shape Design for Elliptic Systems, *Springer-Verlag*, New York, 1984.

[21]J.L. Lions, Optimal Control of Systems Governed by Partial Differential Equations, *Springer-Verlag*, New York, 1971, Translated by S.K. Mitter.

[22]A. Jameson, Optimum Aerodynamic Design Using Control Theory, *Computational Fluid Dynamics Review 1995*, Wiley, 1995.

[23]A. Jameson, L. Martinelli and J. Vassberg, Using CFD for Aerodynamics - A critical Assesment, *Proceedings of ICAS 2002*, September 8-13, 2002, Toronto, Canada

[24]A. Jameson and Sangho Kim, Reduction of the Adjoint Gradient Formula in the Continuous Limit, *AIAA Paper*, 41^{st} AIAA Aerospace Sciences Meeting, Reno January, 2003

[25]E. Ahlstrom, R. Gregg, J. Vassberg, A. Jameson, G-Force: The design of an unlimited Class Reno Racer, *AIAA Paper*, 18^{th} AIAA Applied Aerodynamics Conference, Denver August, 2000

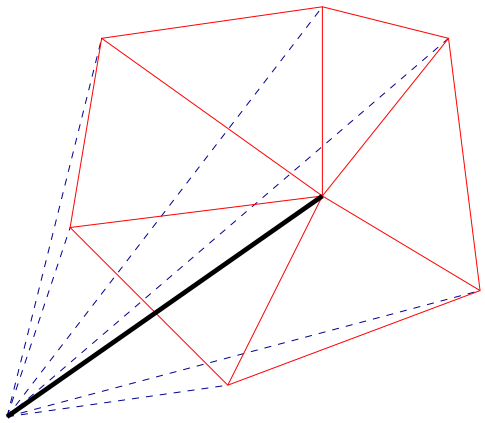

Fig. 1 Control volume for cell-vertex schemes in three dimensions

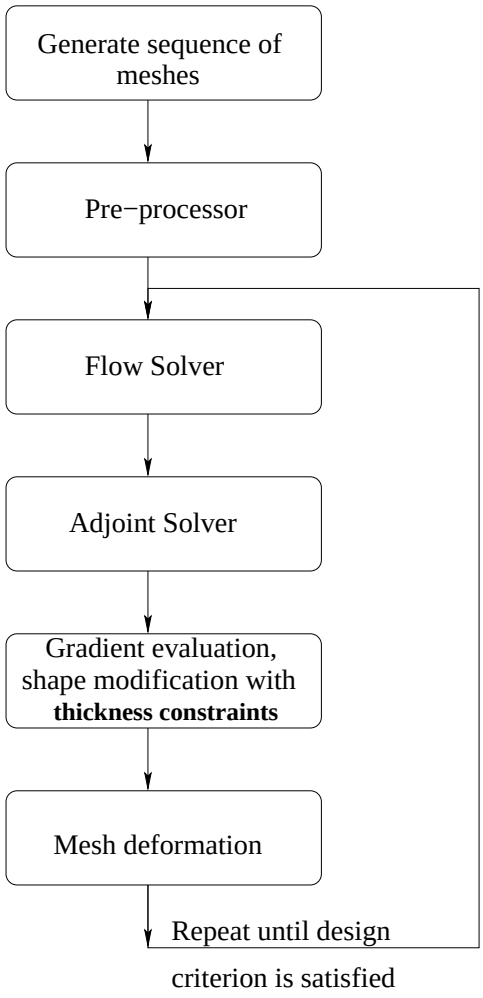

Fig. 3 Flow chart of the overall design process

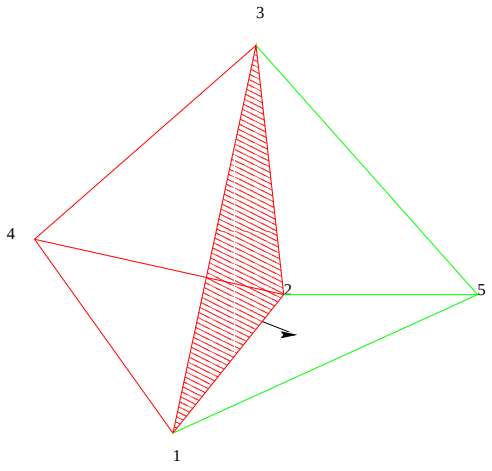

Fig. 2 Evaluation of fluxes in three dimensions

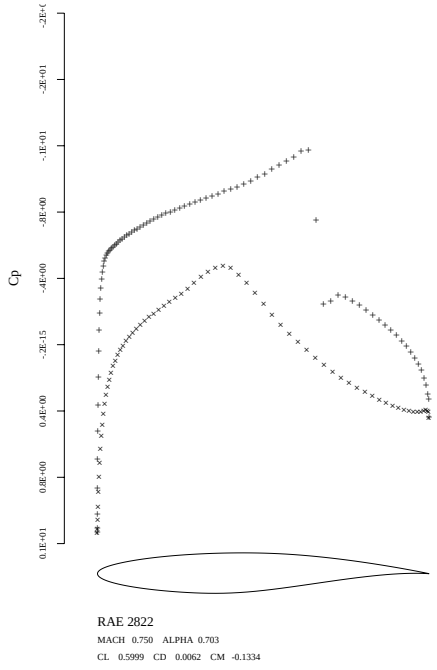

Fig. 4 Initial pressure distribution for the RAE-2822 airfoil

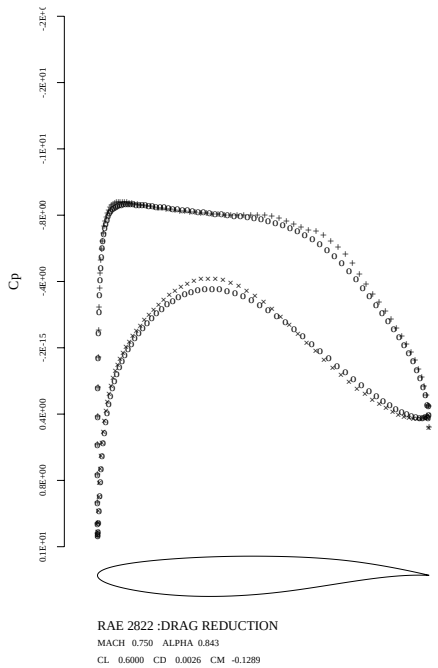

Fig. 5 Pressure distribution as a result of drag minimization for the RAE-2822 airfoil, drag reduced by 36 counts

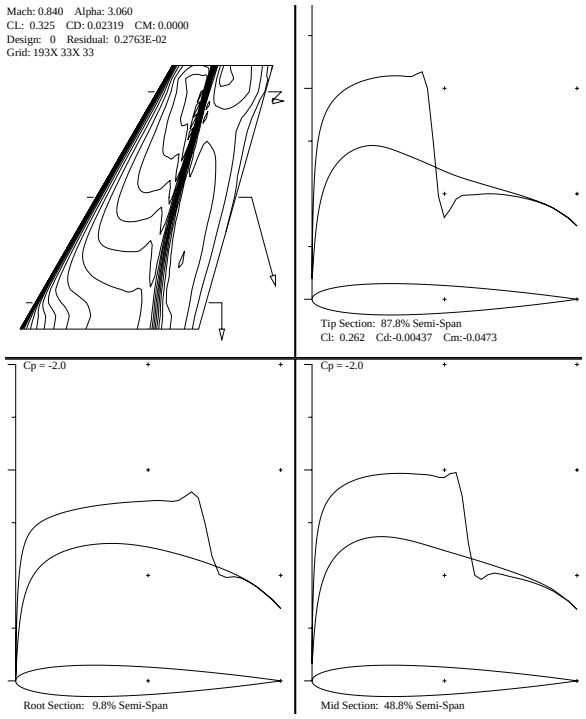

Fig. 7 Initial(dashed lines) and final (solid lines) over a NACA 0012 wing

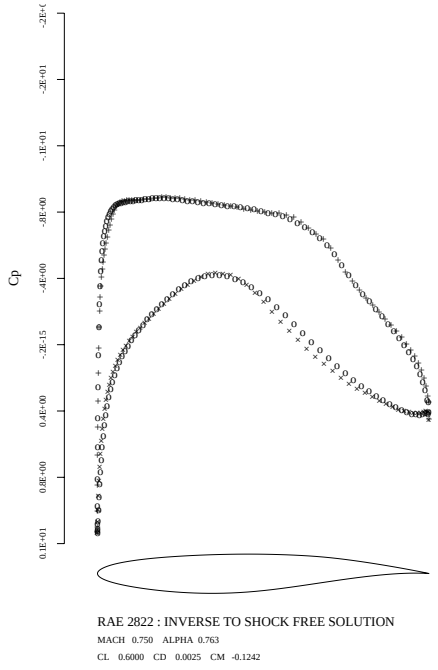

Fig. 6 Attained(+,x) and target(o) pressure distribution for the RAE-2822 airfoil

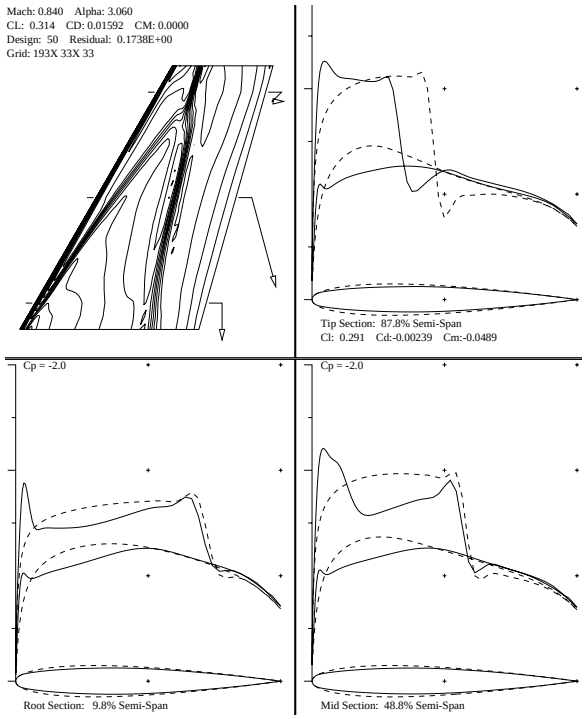

Fig. 8 Initial(dashed lines) and final (solid lines) pressure distribution and modified section geometries

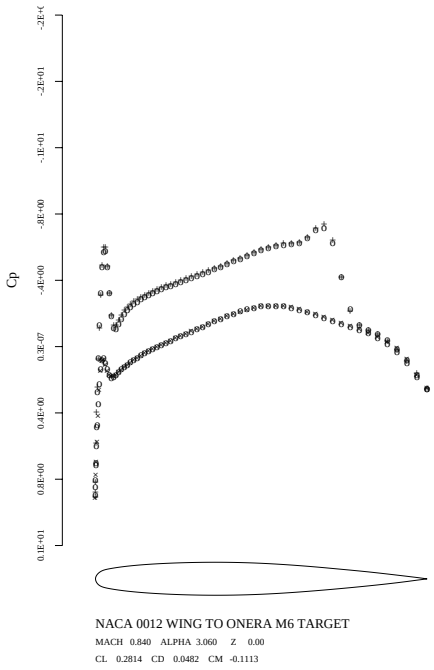

Fig. 9 Attained(+,x) and target(o) pressure distributions at 0 % of the wing span

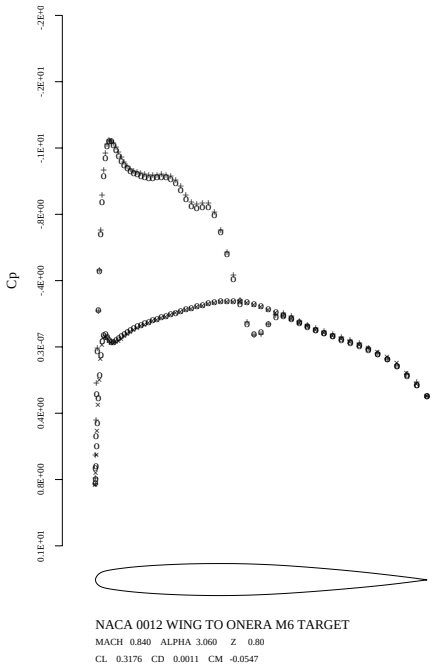

Fig. 11 Attained(+,x) and target(o) pressure distributions at 80 % of the wing span

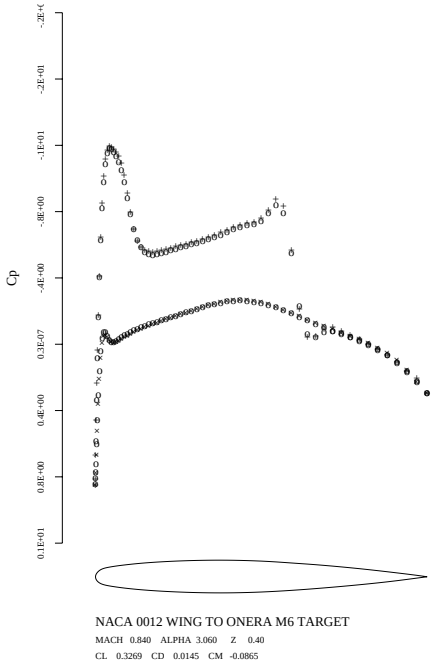

Fig. 10 Attained(+,x) and target(o) pressure distributions at 40 % of the wing span

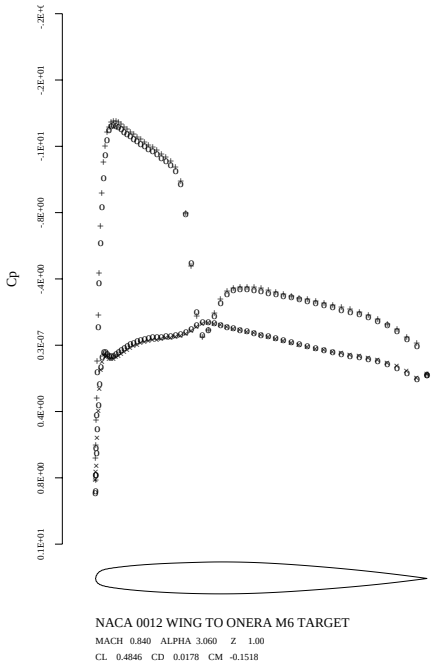

Fig. 12 Final computed and target pressure distributions at 100 % of the wing span

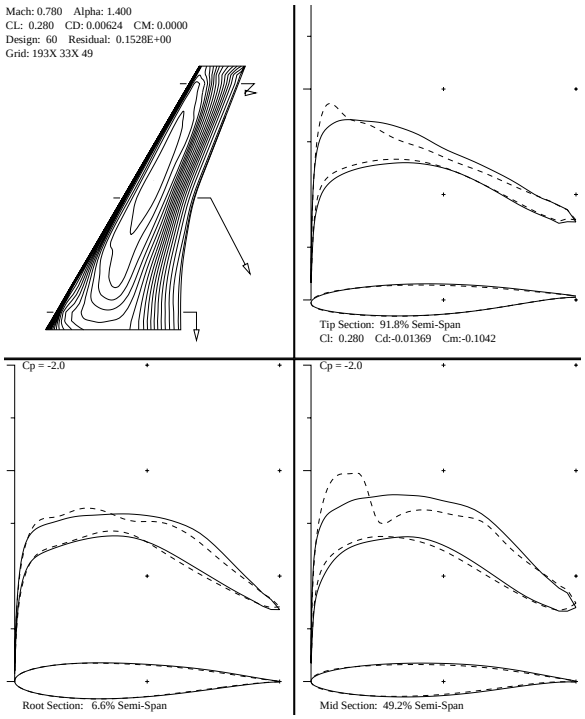

Fig. 13 Initial(dashed lines) and final(solid lines) pressure and section geometries

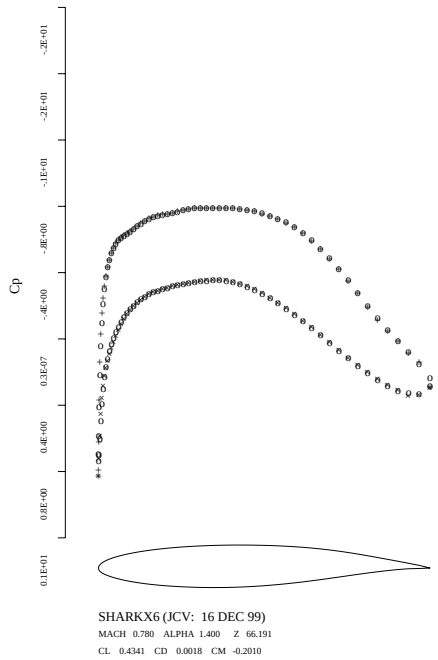

Fig. 15 Attained(+,x) and target(o) pressure distributions at 50 % of the wing span

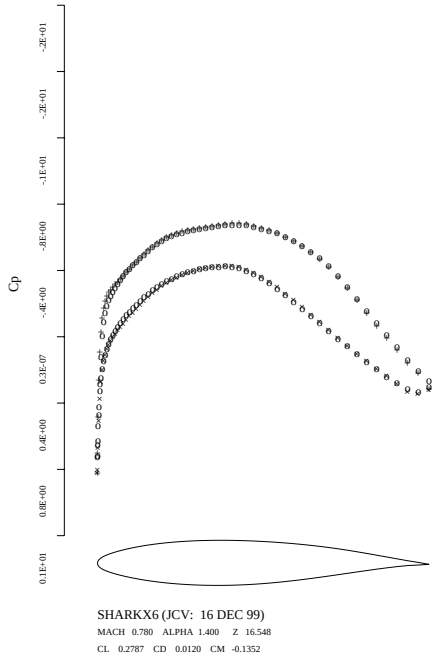

Fig. 14 Attained(+,x) and target(o) pressure distributions at 5 % of the wing span

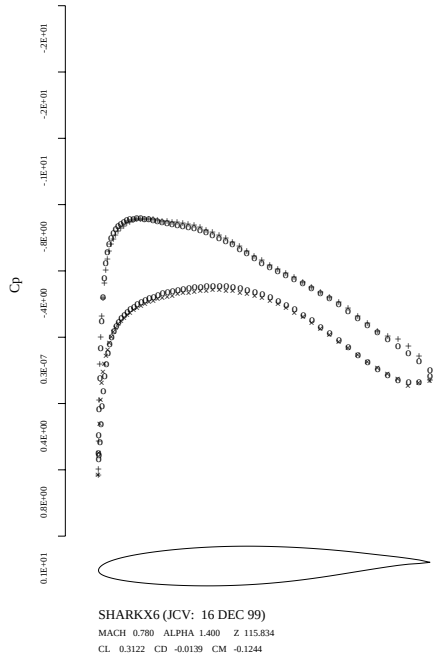

Fig. 16 Initial and final pressure distributions at 95 % of the wing span

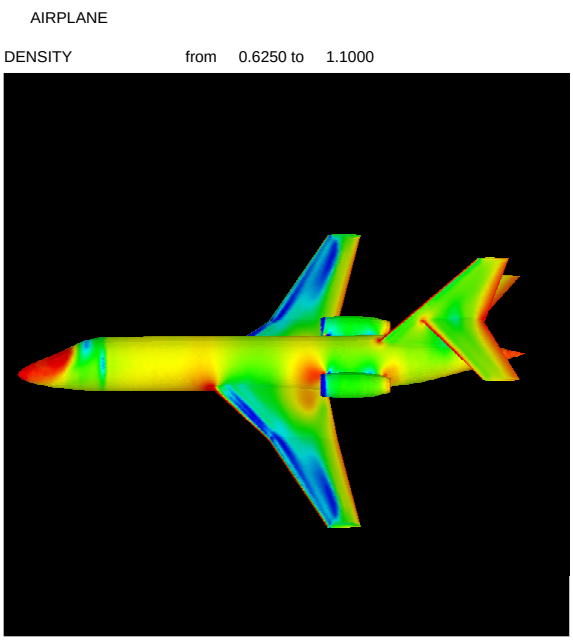

Fig. 17 Density contours for a business jet at $M = 0.8$, $\alpha = 2$

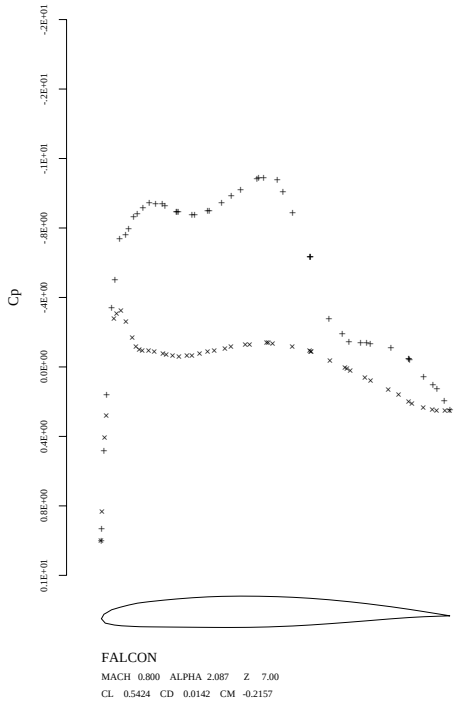

Fig. 19 Pressure distribution at 77 % wing span

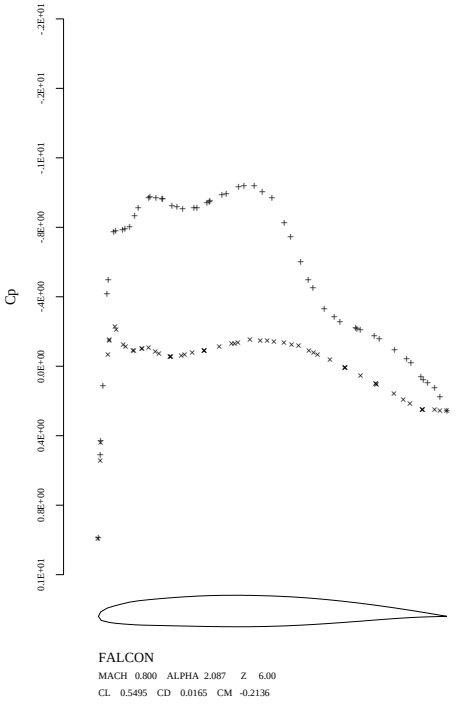

Fig. 18 Pressure distribution at 66 % wing span

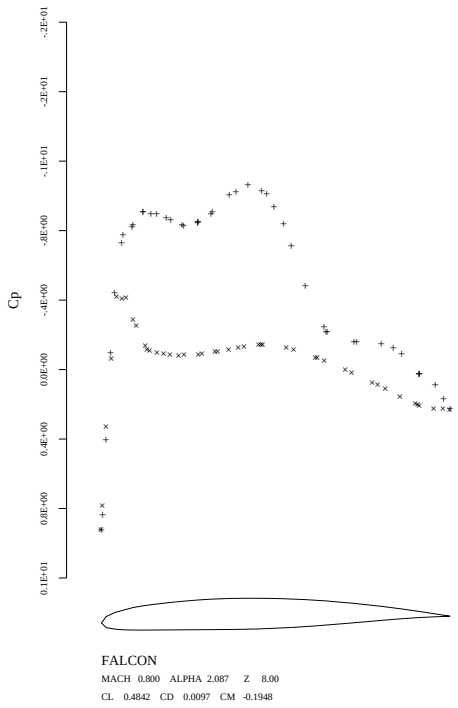

Fig. 20 Pressure distribution at 88 % wing span

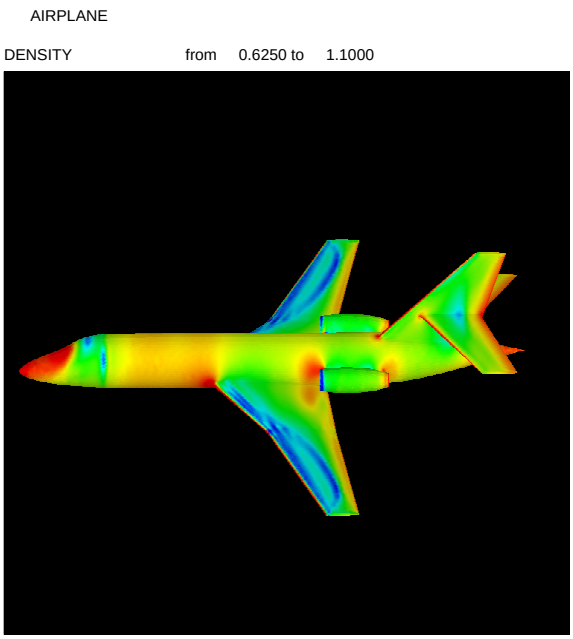

Fig. 21 Density contours for a business jet at $M = 0.8$, $\alpha = 2.3$, after redesign

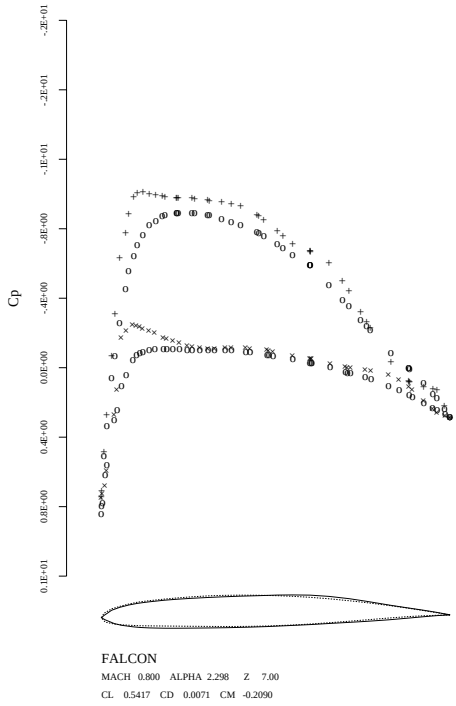

Fig. 23 Pressure distribution at 77 % wing span, after redesign, Dashed line: original geometry, solid line: redesigned geometry

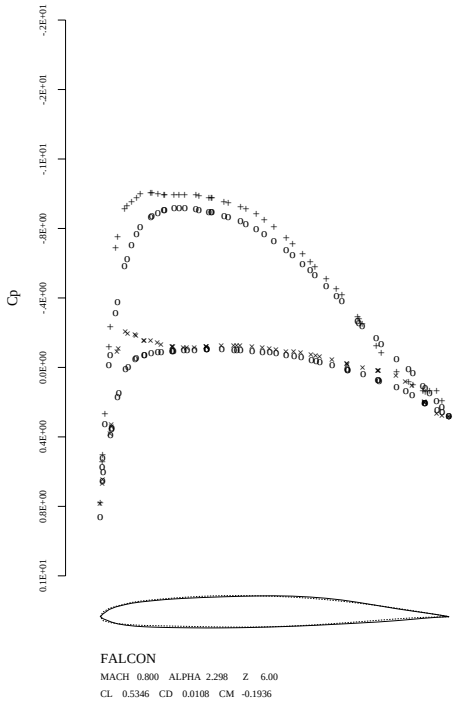

Fig. 22 Pressure distribution at 66 % wing span, after redesign, Dashed line: original geometry, solid line: redesigned geometry

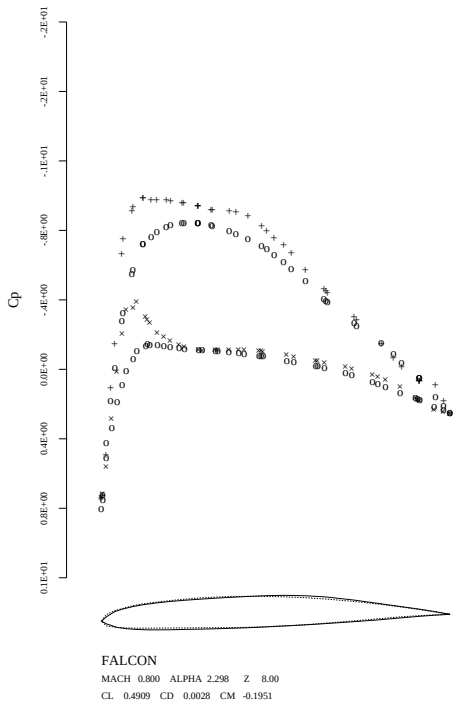

Fig. 24 Pressure distribution at 88 % wing span, after redesign, Dashed line: original geometry, solid line: redesigned geometry

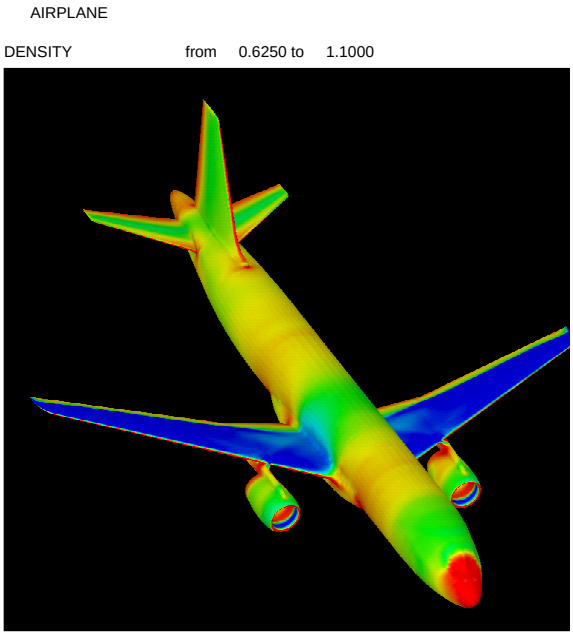

Fig. 25 Density contours for the A-320

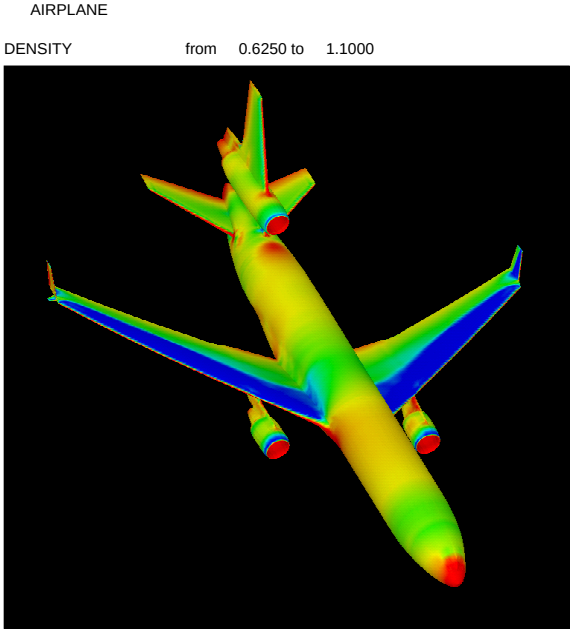

Fig. 26 Density contours for the MD-11

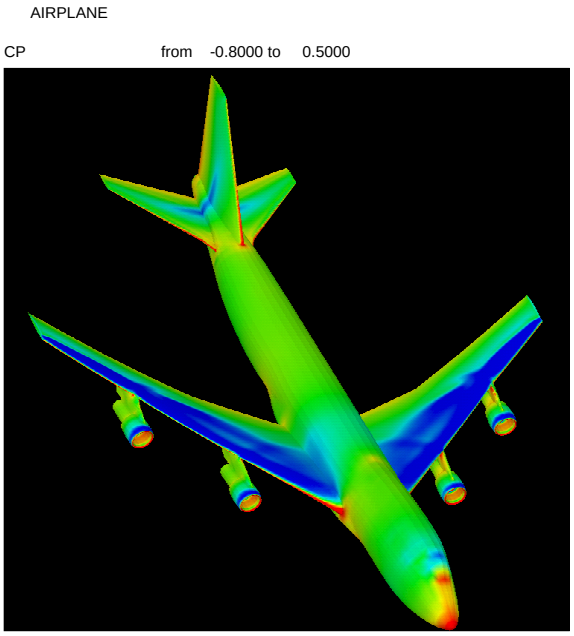

Fig. 27 Pressure contours for the Boeing 747-200

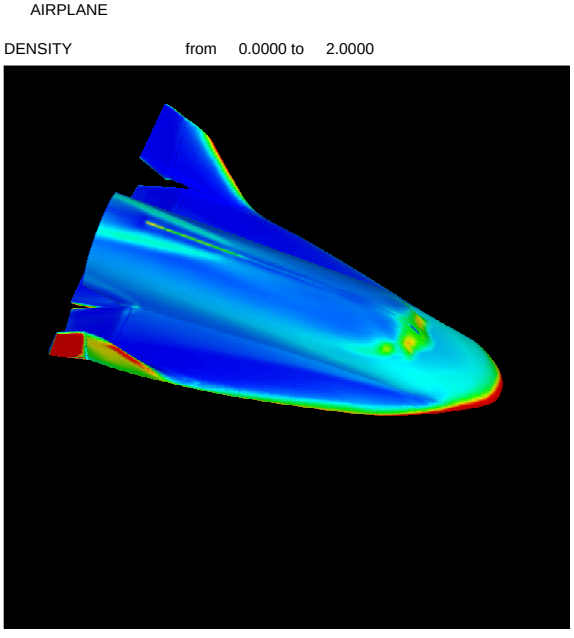

Fig. 28 Pressure contours for the Hermes Shuttle